

# Frequency Adaptability and Waveform Design for OFDM Radar Space-Time Adaptive Processing<sup>†</sup>

Satyabrata Sen, *Member, IEEE* and Charles W. Glover

Center for Engineering Systems Advanced Research

Computer Science and Mathematics Division

Oak Ridge National Laboratory

1 Bethel Valley Road, Oak Ridge, TN 37831-6015, USA

Email: {sens, glovercw}@ornl.gov

Phone: 865-241-9117

**Abstract**— We propose an adaptive waveform design technique for an orthogonal frequency division multiplexing (OFDM) radar signal employing a space-time adaptive processing (STAP) technique. We observe that there are inherent variabilities of the target and interference responses in the frequency domain. Therefore, the use of an OFDM signal can not only increase the frequency diversity of our system, but also improve the target detectability by adaptively modifying the OFDM-coefficients in order to exploit the frequency-variabilities of the scenario. First, we formulate a realistic OFDM-STAP measurement model considering the sparse nature of the target and interference spectra in the spatio-temporal domain. Then, we show that the optimal STAP-filter weight-vector is equal to the generalized eigenvector corresponding to the minimum generalized eigenvalue of the interference and target covariance matrices. With numerical examples we demonstrate that the resultant OFDM-STAP filter-weights are adaptable to the frequency-variabilities of the target and interference responses, in addition to the spatio-temporal variabilities. Hence, by better utilizing the frequency variabilities, we propose an adaptive OFDM-waveform design technique, and consequently gain a significant amount of STAP-performance improvement.

## I. INTRODUCTION

The problem of detecting slowly-moving targets using airborne radars, particularly in the presence of background clutter and hostile electronic countermeasures or jamming, has led to the development of the space-time adaptive processing (STAP) algorithms in the radar community. Since the publication of a seminal paper by Brennan and Reed [1], the STAP techniques have been extensively researched and well-documented in the literature over the last few decades [2]-[7].

In a conventional STAP, for each range gate, the measurements from  $M$  antenna-array elements and  $N$  pulse repetition periods are simultaneously combined to compute the weights of a multidimensional filter. The computation of the optimal (or fully-adaptive) STAP-filter weights requires an inversion of the  $MN \times MN$  interference-only covariance matrix [1], which could be computationally intensive. Moreover, in practical scenarios, the interference is typically unknown a priori and needs to be estimated using the target-free training or secondary data; hence, the approach is known as sample matrix inversion (SMI) [8]. Unfortunately, to achieve a signal-to-interference-plus-noise ratio (SINR) loss within 3 dB of the optimum at

the filter output, at least  $2MN$  homogeneous secondary data are required [8], which might not be available in practice due to the intrinsic nonstationarity of the interference statistics. To tackle these difficulties of a fully-adaptive STAP, several partially-adaptive STAP algorithms are proposed [9]-[12] that can achieve the 3 dB SINR loss performance with only  $2K$  secondary data [13], where  $K \ll MN$  is the number of interfering sources.

In this work, we use a sparsity-based space-time adaptive processing (STAP) algorithm to detect a slowly-moving target using an orthogonal frequency division multiplexing (OFDM) radar. The frequency diversity of the  $L$  orthogonal waveforms (in an  $L$ -subcarrier OFDM system) provides us with additional information about the target. Simultaneously, however, it increases the adaptive degrees-of-freedom (DOFs) of the STAP system to  $LMN$ , and therefore the construction of a fully-adaptive OFDM STAP becomes practically impossible due to the requirement of a larger number of homogeneous secondary data and the computational burden of a bigger matrix inversion. We circumvent these challenges by developing a sparsity-based STAP algorithm that exploits the inherent sparse nature of the energy-distribution of the target and interfering sources in the spatial and temporal domains. Therefore, note here that an OFDM-STAP filter operates on the received data as a whole, in contrast to the subband STAP approach which partitions the data among different subchannels by assuming frequency-independence [14].

First, in Section II, we develop a parametric sparse-measurement model for OFDM radar considering both the clutter and jammer as the interfering sources. Then, in Section III, we describe a residual sparse-recovery technique based on the LASSO estimator [15] to estimate the target and interference covariance matrices, and subsequently compute the optimal STAP-filter weights. To better utilize the frequency-variabilities of the scenario, in Section IV, we propose a simple adaptive OFDM-waveform design technique, in which the OFDM-coefficients are chosen to be in proportional to the measured SINR values at different subcarriers. We present numerical examples in Section V to show the frequency adaptability of the designed STAP-filter weight spectra at different target and interference scenarios and to demonstrate the advantage of waveform design. Finally, concluding remarks are given in Section VI.

<sup>†</sup> This research was partially supported by the Missile Defense Agency (MDA) at the Oak Ridge National Laboratory, managed by UT-Battelle, LLC, for the U.S. Department of Energy, under contract DE-AC05-00OR22725.

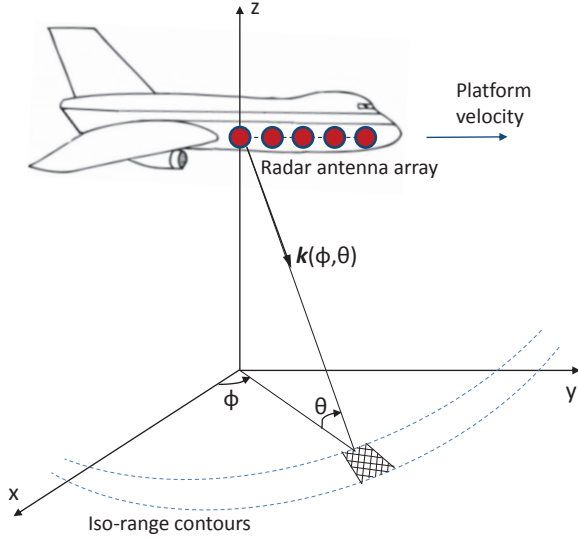


Fig. 1. A schematic representation of the problem scenario.

## II. SPARSE-MEASUREMENT MODEL

Fig. 1 presents a schematic representation of the problem scenario. We consider a radar system residing on an airborne platform and having an  $M$ -element uniformly-spaced linear array (ULA) antenna with inter-element spacing  $d$ . The platform is flying at a fixed height  $H$  and with a constant velocity  $\mathbf{v}_r$  along the  $y$ -direction. The axis of the ULA is oriented along the direction of the platform movement (this is commonly known as the sidelooking array configuration [3, Ch. 2]). Without loss of generality, we assume that the array elements are identical and have omnidirectional radiation patterns. The chosen co-ordinate system is also depicted in Fig. 1. We define the  $x$ -direction as the zero azimuth (i.e.,  $\phi = 0^\circ$ ) and the  $xy$ -plane as the zero elevation (i.e.,  $\theta = 0^\circ$ ). Therefore, a unit vector  $\mathbf{k}$  pointing towards a patch on the ground at the  $(\phi, \theta)$  direction can be expressed as  $\mathbf{k}(\phi, \theta) = \cos \phi \cos \theta \hat{\mathbf{x}} + \sin \phi \cos \theta \hat{\mathbf{y}} + \sin \theta \hat{\mathbf{z}}$ , where  $\hat{\mathbf{x}}$ ,  $\hat{\mathbf{y}}$ , and  $\hat{\mathbf{z}}$  are the standard unit vectors of the Cartesian co-ordinate system.

We consider a wideband OFDM signaling system with  $L$  active subcarriers, a bandwidth of  $B$  Hz, and pulse duration of  $T$  seconds. Let  $\mathbf{a} = [a_0, a_1, \dots, a_{L-1}]^T$  represent the complex weights transmitted over the  $L$  subcarriers, and satisfying  $\sum_{l=0}^{L-1} |a_l|^2 = 1$ . In the next few subsections, we elaborate on the sparse modeling of the resulting measurement vector by considering the individual contribution from the target, clutter, jammer, and thermal noise, and also state the associated statistical assumptions.

1) *Target*: We consider the target as a far-field point scatterer at distance  $r_0$ , direction  $(\phi_T, \theta_T)$ , and is moving with velocity  $\mathbf{v}_T$ . The distance  $r_0$  corresponds to a specific range gate (that is under test), denoted by a roundtrip delay  $\tau_0 = 2r_0/c$ , where  $c$  is the speed of propagation. Then, in the absence of any other interfering signals or noise, we can express the target space-time snapshot at the output of the  $l$ th

subchannel as

$$\mathbf{y}_T(l) = \zeta_{T,l} \mathbf{a}_l \phi(\alpha_l, \nu_l), \quad (1)$$

where  $\zeta_{T,l}$  is a complex quantity representing the target-scattering coefficient at the  $l$ th subchannel and

$$\phi(\alpha_l, \nu_l) = \mathbf{f}_D(\nu_l) \otimes \mathbf{f}_S(\alpha_l) \quad (2)$$

is an  $MN \times 1$  space-time steering vector with

$$\mathbf{f}_D(\nu_l) = [1, e^{j2\pi\nu_l}, \dots, e^{j2\pi(N-1)\nu_l}]^T, \quad (3)$$

$$\mathbf{f}_S(\alpha_l) = e^{-j2\pi f_l \tau_0} \cdot [1, e^{j2\pi\alpha_l}, \dots, e^{j2\pi(M-1)\alpha_l}]^T, \quad (4)$$

representing the Doppler (or temporal) and spatial steering vectors, respectively. The normalized spatial frequency  $\alpha_l$  and normalized Doppler frequency  $\nu_l$  are respectively defined as

$$\alpha_l = f_l \gamma \Delta\tau, \quad \nu_l = f_l \beta T, \quad (5)$$

where  $\gamma = 1 + \beta$  accounts for the stretching or compressing in time of the reflected signal due to the relative motion between the radar and target;  $\beta = 2\langle(\mathbf{v}_r - \mathbf{v}_T), \mathbf{k}\rangle/c$  is the relative Doppler shift;  $\Delta\tau = \langle d\hat{\mathbf{y}}, \mathbf{k}\rangle/c$  is the inter-element time-delay; and  $T$  is the pulse repetition interval (PRI). However, note that in most of the practical scenarios  $|\beta| \ll 1$ , and therefore  $\gamma = 1 + \beta \approx 1$  in (5).

Now, suppose instead of a specific pair of  $(\alpha_l, \nu_l)$ , we consider all the possible combinations of  $(\alpha_{l,i}, \nu_{l,j})$  for  $i = 1, 2, \dots, G_\alpha$  and  $j = 1, 2, \dots, G_\nu$ . In other words, we discretize the spatio-temporal domain into  $G \triangleq G_\alpha G_\nu$  grid points, where  $G_\alpha$  and  $G_\nu$  are the number of grids along the spatial and temporal axes, respectively. Then, a nonzero content from any such grid point would suggest the presence of a scatterer at that particular spatial and temporal frequencies. Hence, we can rewrite (1) as

$$\mathbf{y}_T(l) = \mathbf{a}_l \Phi_l \mathbf{x}_{T,l}, \quad (6)$$

where  $\Phi_l = [\phi_l(1, 1) \ \phi_l(1, 2) \ \dots \ \phi_l(G_\alpha, G_\nu)]$  is an  $MN \times G$  matrix containing all the possible combinations of spatial and Doppler steering vectors (for notational simplicity we write  $\phi(\alpha_{l,i}, \nu_{l,j})$  as  $\phi_l(i, j)$ ); and  $\mathbf{x}_{T,l}$  is a  $G \times 1$  sparse vector having only one nonzero entry corresponding to the target response at the true spatial and Doppler frequencies (computed using  $\phi_T$ ,  $\theta_T$ , and  $\mathbf{v}_T$ ). Then, stacking all the  $\mathbf{y}_T(l)$ s, we get the overall target space-time snapshot as

$$\mathbf{y}_T = \Psi_A \mathbf{x}_T, \quad (7)$$

where  $\mathbf{y}_T = [\mathbf{y}_T(0)^T, \mathbf{y}_T(1)^T, \dots, \mathbf{y}_T(L-1)^T]^T$ ;  $\Psi_A = \text{blkdiag}(\mathbf{a}_0 \Phi_0, \mathbf{a}_1 \Phi_1, \dots, \mathbf{a}_{L-1} \Phi_{L-1})$  is an  $LMN \times LG$  sparse spatio-temporal measurement matrix, with the subscript 'A' suggesting the active mode of radar operation; and  $\mathbf{x}_T = [\mathbf{x}_{T,0}^T, \dots, \mathbf{x}_{T,L-1}^T]^T$  is an  $LG \times 1$  sparse vector having only  $L$  nonzero entries that are equal to the actual target-scattering coefficients,  $[\zeta_{T,0}, \dots, \zeta_{T,L-1}]^T$ , at the  $L$  subchannels.

We assume that the scattering coefficients of the target represent zero-mean random complex numbers and are correlated

among different subchannels. Therefore, the target space-time covariance matrix is given by

$$\mathbf{R}_T = \sum_{g_1, g_2 \in \mathcal{T}} E \left( x_{T, g_1} x_{T, g_2}^* \right) \boldsymbol{\psi}_{A, g_1} \boldsymbol{\psi}_{A, g_2}^H, \quad (8)$$

where  $\mathcal{T} = \text{supp}(\mathbf{x}_T) \subseteq \{1, 2, \dots, LG\}$  denotes the support-set of  $\mathbf{x}_T$ , i.e., the set of indices corresponding to the nonzero entries of  $\mathbf{x}_T$ ;  $x_{T, g_1}$ ,  $x_{T, g_2}$  are the  $g_1$ th,  $g_2$ th entries in  $\mathbf{x}_T$ ; and  $\boldsymbol{\psi}_{A, g_1}$ ,  $\boldsymbol{\psi}_{A, g_2}$  are the  $g_1$ th,  $g_2$ th columns of  $\boldsymbol{\Psi}_A$ .

2) *Clutter*: For an airborne radar, the main contribution to the clutter originates due to the ground reflections from all the azimuth directions. Though the ground has zero velocity, the ground-clutter is spread in both the angle and Doppler frequency due to the platform velocity  $\mathbf{v}_R$ . To model in an amenable way, we represent the clutter returns (from a particular range gate) as a coherent summation of a large number ( $N_c$ ) of clutter patches evenly distributed in azimuth angles  $\phi_k$ ,  $k = 1, 2, \dots, N_c$ . Then, noticing that the target and clutter returns are affected in a similar way by the radar transmission, we follow the same approach presented in the previous subsection to construct a sparse representation of the clutter space-time snapshot as

$$\mathbf{y}_C = \sum_{k=1}^{N_c} \boldsymbol{\Psi}_A \mathbf{x}_{C, k} = \boldsymbol{\Psi}_A \mathbf{x}_C, \quad (9)$$

where  $\mathbf{x}_{C, k}$  is an  $LG \times 1$  sparse vector having  $L$  nonzero entries that correspond to the clutter returns from a specific azimuth angle  $\phi_k$ ; and  $\mathbf{x}_C$  is another  $LG \times 1$  sparse vector with sparsity level  $LN_c$ , and representing the overall clutter response.

We assume that the clutter returns are also zero-mean random complex numbers, and similar to (8) the clutter space-time covariance matrix is given by

$$\mathbf{R}_C = \sum_{g_1, g_2 \in \mathcal{C}} E \left( x_{C, g_1} x_{C, g_2}^* \right) \boldsymbol{\psi}_{A, g_1} \boldsymbol{\psi}_{A, g_2}^H, \quad (10)$$

where  $\mathcal{C} = \text{supp}(\mathbf{x}_C) \subseteq \{1, 2, \dots, LG\}$  denotes the support-set of  $\mathbf{x}_C$ ; and  $x_{C, g_1}$ ,  $x_{C, g_2}$  are the  $g_1$ th,  $g_2$ th entries of  $\mathbf{x}_C$ . Conventionally, however, the clutter returns from different patches are assumed to be uncorrelated.

3) *Jammer*: The jamming signals produce noise-like responses from certain directions onto the radar receiver. Considering a jamming signal arriving at the radar from the direction  $(\phi_J, \theta_J)$ , we can model the jammer space-time snapshot at the  $l$ th subchannel as

$$\mathbf{y}_J(l) = \boldsymbol{\zeta}_{J, l} \otimes \mathbf{f}_S(\alpha_l) = \mathbf{F}(\alpha_l) \boldsymbol{\zeta}_{J, l}, \quad (11)$$

where  $\boldsymbol{\zeta}_{J, l} = [\zeta_{J, l}(0), \zeta_{J, l}(1), \dots, \zeta_{J, l}(N-1)]^T$  is the jammer response at the  $l$ th subchannel and  $N$  pulse repetition periods;  $\mathbf{f}_S(\alpha_l)$  is the jammer steering vector, computed using  $(\phi_J, \theta_J)$ ; and  $\mathbf{F}(\alpha_l) = \text{blkdiag}(\mathbf{f}_S(\alpha_l), \mathbf{f}_S(\alpha_l), \dots, \mathbf{f}_S(\alpha_l))$  is an  $MN \times N$  matrix.

Then, we discretize only the spatial domain into  $G_\alpha$  grid points  $\{\alpha_{l, i}, i = 1, 2, \dots, G_\alpha\}$ , and construct a sparse representation of the jammer space-time snapshot as

$$\mathbf{y}_J = \boldsymbol{\Psi}_P \mathbf{x}_J, \quad (12)$$

where  $\mathbf{y}_J = [\mathbf{y}_J(0)^T, \mathbf{y}_J(1)^T, \dots, \mathbf{y}_J(L-1)^T]^T$ ;  $\boldsymbol{\Psi}_P = \text{blkdiag}(\mathbf{F}_0, \mathbf{F}_1, \dots, \mathbf{F}_{L-1})$  is an  $LMN \times LG_\alpha N$  sparse spatial measurement matrix, and to distinguish it from  $\boldsymbol{\Psi}_A$  we use the subscript 'P' that implies the passive mode of radar operation;  $\mathbf{F}_l = [\mathbf{F}_l(1) \mathbf{F}_l(2) \dots \mathbf{F}_l(G_\alpha)]$  is an  $MN \times G_\alpha N$  matrix containing all the possible spatial frequencies; and  $\mathbf{x}_J = [\mathbf{x}_{J, 0}^T, \dots, \mathbf{x}_{J, L-1}^T]^T$  is an  $LG_\alpha N \times 1$  sparse vector having  $LN_J N$  nonzero entries when  $N_J$  jammers are present.

The jammer responses are also assumed to be zero-mean complex numbers having the space-time covariance matrix

$$\mathbf{R}_J = \sum_{g_1, g_2 \in \mathcal{J}} E \left( x_{J, g_1} x_{J, g_2}^* \right) \boldsymbol{\psi}_{P, g_1} \boldsymbol{\psi}_{P, g_2}^H, \quad (13)$$

where  $\mathcal{J} = \text{supp}(\mathbf{x}_J) \subseteq \{1, 2, \dots, LG_\alpha N\}$  is the nonzero support of  $\mathbf{x}_J$ ; as before  $x_{J, g_1}$ ,  $x_{J, g_2}$  are the  $g_1$ th,  $g_2$ th entries of  $\mathbf{x}_J$ ; and  $\boldsymbol{\psi}_{P, g_1}$ ,  $\boldsymbol{\psi}_{P, g_2}$  are the  $g_1$ th,  $g_2$ th columns of  $\boldsymbol{\Psi}_P$ .

4) *Noise*: We assume that the contribution of the noise component originates only from the receiver generated thermal noise. Conventionally, the noise components are considered to be both spatially and temporally uncorrelated. We further assume that the noise is uncorrelated among different subchannels. Then, denoting  $\sigma_e^2$  as the noise power per sensor element per subchannel, we can write the space-time covariance matrix of the noise component as

$$\mathbf{R}_e = E(\mathbf{e} \mathbf{e}^H) = \sigma_e^2 \mathbf{I}_{LMN}. \quad (14)$$

Finally, based on the assumption of additive contributions from the target, clutter, jammer, and thermal noise signals, we get the overall measurement model as

$$\mathbf{y} = \mathbf{y}_T + \mathbf{y}_C + \mathbf{y}_J + \mathbf{e} = \boldsymbol{\Psi}_A \mathbf{x}_T + \boldsymbol{\Psi}_A \mathbf{x}_C + \boldsymbol{\Psi}_P \mathbf{x}_J + \mathbf{e}, \quad (15)$$

and the mutual uncorrelatedness among these components results in the overall covariance matrix as

$$\mathbf{R} = E(\mathbf{y} \mathbf{y}^H) = \mathbf{R}_T + \mathbf{R}_I, \quad (16)$$

where  $\mathbf{R}_I = \mathbf{R}_C + \mathbf{R}_J + \mathbf{R}_e$  is the total interference covariance matrix.

### III. SPACE-TIME ADAPTIVE PROCESSING FILTER DESIGN

In STAP, the received data  $\mathbf{y}$  is processed with a linear filter having weights  $\mathbf{w}$  to yield a scalar output

$$z = \mathbf{w}^H \mathbf{y}, \quad (17)$$

which is then compared with a pre-defined threshold to decide about the presence of a target-of-interest. The threshold is determined to achieve a specified probability of false alarm ( $P_{FA}$ ) of a decision problem that chooses one of the two possible hypotheses: the null hypothesis  $\mathcal{H}_0$  with  $\mathbf{y} = \mathbf{y}_C + \mathbf{y}_J + \mathbf{e}$  (target-free hypothesis) or the alternate hypothesis  $\mathcal{H}_1$  with  $\mathbf{y} = \mathbf{y}_T + \mathbf{y}_C + \mathbf{y}_J + \mathbf{e}$  (target-present hypothesis). For such a detection problem with constant  $P_{FA}$  and assuming that the interference and noise processes are Gaussian, the primary objective of a STAP-filter design is to maximize probability of detection ( $P_D$ ) by maximizing the SINR at the filter output:

$$\text{SINR} = \frac{\mathbf{w}^H \mathbf{R}_T \mathbf{w}}{\mathbf{w}^H \mathbf{R}_I \mathbf{w}}. \quad (18)$$

Now, following the approach presented in [8] and defining an inner product  $\langle \mathbf{w}_1, \mathbf{w}_2 \rangle \triangleq \mathbf{w}_1^H \mathbf{R}_1 \mathbf{w}_2$  with respect to the positive-definite Hermitian matrix  $\mathbf{R}_1$ , we have

$$\begin{aligned} \text{SINR} &= \frac{\langle \mathbf{w}, \mathbf{R}_1^{-1} \mathbf{R}_T \mathbf{w} \rangle}{\langle \mathbf{w}, \mathbf{w} \rangle}, \\ &\leq \frac{[\langle \mathbf{w}, \mathbf{w} \rangle \langle \mathbf{R}_1^{-1} \mathbf{R}_T \mathbf{w}, \mathbf{R}_1^{-1} \mathbf{R}_T \mathbf{w} \rangle]^{\frac{1}{2}}}{\langle \mathbf{w}, \mathbf{w} \rangle}, \\ &= \left[ \frac{\mathbf{w}^H \mathbf{R}_T^H \mathbf{R}_1^{-1} \mathbf{R}_T \mathbf{w}}{\mathbf{w}^H \mathbf{R}_1 \mathbf{w}} \right]^{\frac{1}{2}}. \end{aligned} \quad (19)$$

Here, the second inequality follows from the Cauchy-Schwarz inequality. Hence, the maximum SINR can be attained when

$$\mathbf{w} = \lambda \mathbf{R}_1^{-1} \mathbf{R}_T \mathbf{w}, \quad \text{i.e.,} \quad \mathbf{R}_1 \mathbf{w} = \lambda \mathbf{R}_T \mathbf{w}, \quad (20)$$

where  $\lambda$  is a constant not equal to zero. Equation (20) is the generalized eigenvalue-eigenvector formulation for the pair of matrices  $(\mathbf{R}_1, \mathbf{R}_T)$ . Substituting (20) into (19), it can be shown that

$$\text{SINR} \leq \left[ \frac{\mathbf{w}^H \mathbf{R}_T^H \mathbf{R}_1^{-1} \mathbf{R}_T \mathbf{w}}{\mathbf{w}^H \mathbf{R}_1 \mathbf{w}} \right]^{\frac{1}{2}} = \frac{1}{\lambda}, \quad (21)$$

and hence we select the optimal STAP-filter weight-vector as the generalized eigenvector corresponding to the minimum generalized eigenvalue of  $(\mathbf{R}_1, \mathbf{R}_T)$ .

In practical scenarios, the knowledge of  $\mathbf{R}_1$  and  $\mathbf{R}_T$  are unknown to the radar receiver, and therefore they are need to be estimated from the measurements of the primary and secondary range gates. To efficiently estimate the covariance matrices  $\mathbf{R}_1$  and  $\mathbf{R}_T$ , we first employ the LASSO estimator as a sparse-recovery technique to obtain the estimates of  $\mathbf{x}_T$ ,  $\mathbf{x}_C$ , and  $\mathbf{x}_J$ , and then pre-multiply them with the known sparse measurement matrices  $\Psi_A$  and  $\Psi_P$ .

First, we operate the radar in the passive mode to find an estimate of  $\mathbf{x}_J$  using the target-free and clutter-free jamming signals,  $\mathbf{y}_p = \Psi_P \mathbf{x}_J + \mathbf{e}_p$ , as

$$\hat{\mathbf{x}}_J = \arg \min_{\mathbf{x}_J} \|\mathbf{y}_p - \Psi_P \mathbf{x}_J\|_2^2 + \epsilon_J \|\mathbf{x}_J\|_1, \quad (22)$$

where  $\epsilon_J$  is a regularization parameter. Subsequently, an estimate of the jammer covariance matrix is computed as

$$\hat{\mathbf{R}}_J = \sum_{g_1, g_2 \in \hat{\mathcal{J}}} \left( \hat{x}_{J, g_1} \hat{x}_{J, g_2}^* \right) \psi_{P, g_1} \psi_{P, g_2}^H, \quad (23)$$

where  $\hat{\mathcal{J}}$  is the support-set of the estimated jammer response.

Next, we find an estimate of  $\mathbf{x}_{C, s}$  from the residual secondary measurements,  $\{\check{\mathbf{y}}_s = \Psi_A \mathbf{x}_{C, s} + \Psi_P \mathbf{x}_{J, s} + \mathbf{e}_s - \Psi_P \hat{\mathbf{x}}_J, s = 1, 2, \dots, N_s\}$ , as

$$\hat{\mathbf{x}}_{C, s} = \arg \min_{\mathbf{x}_{C, s}} \|\check{\mathbf{y}}_s - \Psi_A \mathbf{x}_{C, s}\|_2^2 + \epsilon_C \|\mathbf{x}_{C, s}\|_1, \quad (24)$$

where  $\epsilon_C$  is a tuning parameter. Then, we estimate the clutter covariance matrix as

$$\hat{\mathbf{R}}_C = \frac{1}{N_s} \sum_{s=1}^{N_s} \left[ \sum_{g_1, g_2 \in \hat{\mathcal{C}}_s} \left( \hat{x}_{C, s, g_1} \hat{x}_{C, s, g_2}^* \right) \psi_{A, g_1} \psi_{A, g_2}^H \right], \quad (25)$$

where  $\hat{\mathcal{C}}_s$  is the nonzero support-set of the estimated clutter response from the  $s$ th secondary data. Hence, using (23) and (25), the estimate of the overall interference covariance matrix is given by

$$\hat{\mathbf{R}}_I = \hat{\mathbf{R}}_C + \hat{\mathbf{R}}_J + \eta \mathbf{I}_{LMN}, \quad (26)$$

where  $\eta$  is a positive constant.

Similarly, we use the residual primary measurement,  $\check{\mathbf{y}} = \Psi_A \mathbf{x}_T + \Psi_A \mathbf{x}_C + \Psi_P \mathbf{x}_J + \mathbf{e} - \Psi_A \hat{\mathbf{x}}_C - \Psi_P \hat{\mathbf{x}}_J$  where  $\hat{\mathbf{x}}_C = (1/N_s) \sum_{s=1}^{N_s} \hat{\mathbf{x}}_{C, s}$ , to obtain

$$\hat{\mathbf{x}}_T = \arg \min_{\mathbf{x}_T} \|\check{\mathbf{y}} - \Psi_A \mathbf{x}_T\|_2^2 + \epsilon_T \|\mathbf{x}_T\|_1, \quad (27)$$

where  $\epsilon_T$  is a controlling parameter. An estimate of the target covariance matrix is evaluated as

$$\hat{\mathbf{R}}_T = \sum_{g_1, g_2 \in \hat{\mathcal{T}}} \left( \hat{x}_{T, g_1} \hat{x}_{T, g_2}^* \right) \psi_{A, g_1} \psi_{A, g_2}^H, \quad (28)$$

where  $\hat{\mathcal{T}}$  denotes the support-set of the estimated target response.

Finally, substituting (26) and (28) into (20), we find the optimal STAP-filter weight-vector as the generalized eigenvector corresponding to the minimum generalized eigenvalue of the matrix pair  $(\hat{\mathbf{R}}_I, \hat{\mathbf{R}}_T)$ .

#### IV. FREQUENCY ADAPTABILITY AND WAVEFORM DESIGN

The term ‘‘adaptive’’ in the standard STAP literature implies the adaptation capability of the filter-weights in accordance to the target and interference characteristics in the spatial and temporal domains. However, in OFDM-STAP, the construction of the filter weights according to (20) further makes them adaptable to the frequency variabilities of target and interference responses. The variations in the designed STAP-filter weights change with respect to the target and interference variabilities in a ‘‘waterfilling’’ type approach - allowing easy target-detectability along the subcarrier at which the target response is stronger, while simultaneously blocking the interfering signals along some other subcarriers at which the target response is weaker. We demonstrate this aspect with numerical examples in the next section.

The inherent variabilities present in the frequency domain motivate us to propose an adaptive waveform design technique in order to further improve the STAP performance. Depending on the frequency-variability of the SINR values, computed from the designed filter-weights and estimated covariance matrices at the current CPI, we design the transmitting OFDM-spectrum for the next CPI. We select the OFDM-coefficients,  $a_l$ s, to be in proportional to the measured SINR values at respective subcarriers, i.e.,

$$a_l = \rho \frac{\mathbf{w}_l^H \hat{\mathbf{R}}_{T, l} \mathbf{w}_l}{\mathbf{w}_l^H \hat{\mathbf{R}}_{I, l} \mathbf{w}_l}, \quad (29)$$

where  $\rho$  is a normalizing constant to satisfy the total transmitted-power constraint  $\sum_{l=0}^{L-1} |a_l|^2 = 1$ ;  $\mathbf{w}_l$  is an  $MN \times 1$  vector representing the evaluated filter-weight at the  $l$ th subcarrier; and  $\hat{\mathbf{R}}_{T, l}$ ,  $\hat{\mathbf{R}}_{I, l}$  are the  $MN \times MN$  submatrices at the

$(l, l)$ th block-index of the target and interference covariance matrices, respectively.

## V. NUMERICAL RESULTS

In this section, we present the results of several numerical examples to illustrate the frequency adaptability of the designed STAP-filter weights and to demonstrate the advantage of waveform design. We simulated the situation of a range gate that was at a distance of  $R = 10$  km from the radar. The target was at  $\phi_T = 0^\circ$  and was moving with  $v_T = 25$  m/s. The scattering coefficients of the target were generated from a zero-mean complex Gaussian distribution having covariance matrix  $\Sigma_T$ , and then scaled accordingly to satisfy the specific signal-to-noise ratio (SNR). The clutter and jammer responses were also generated from independent zero-mean complex Gaussian distributions, and subsequently scaled to satisfy the required clutter-to-noise ratio (CNR) and jammer-to-noise ratio (JNR), respectively. The clutter responses were assumed to be equally spaced in azimuth angles over the entire range gate, and there were two jamming sources at  $\phi_j^{(1)} = -30^\circ$  and  $\phi_j^{(2)} = 60^\circ$ . The radar was at a height  $H = 5$  km and moving with  $v_R = 100$  m/s along the  $y$ -direction (see Fig. 1). It used a linear array with  $M = 10$  sensor elements and a CPI having  $N = 8$  temporal pulses. The radar employed an  $L = 3$  subcarrier OFDM signaling scheme with the following parameters: carrier frequency  $f_c = 1$  GHz; bandwidth  $B = 100$  MHz; subcarrier spacing  $\Delta f = B/(L + 1) = 20$  MHz; pulse width  $T_p = 1/\Delta f = 50$  ns; pulse repetition interval  $T = 10$  ms; and all the transmitted OFDM coefficients were equal, i.e.,  $\mathbf{a} = (1/\sqrt{L})\mathbf{1}_L$ .

To show the frequency adaptability of the designed STAP-filter weights, we designed three different target scenarios by varying the target powers across different subcarriers but keeping the interference-plus-noise powers the same. We ensured that the total SNR remained constant at 30 dB, while the CNR and JNR values were at 40 dB. In Scenario 1, we had equal target powers at the three subcarriers with  $\Sigma_T^{(1)} = [1, 0.1, 0.01; 0.1, 1, 0.1; 0.01, 0.1, 1]$ , and hence the resultant weight-spectra in Fig. 2(a) show approximately equivalent spatio-temporal behaviors. We considered a varying target response in Scenario 2, with the strongest reflectivity along the second subcarrier, as  $\Sigma_T^{(2)} = [2, 0.28, 0.14; 0.28, 4, 0.2; 0.14, 0.2, 1]$ , and the resulting weight-spectra are depicted in Fig. 2(b). We observe that the spatio-temporal patterns of the filter-weights at different subcarriers adjust themselves accordingly, allowing a prominent peak only at the second subcarrier to detect the target. Importantly, we notice a lot more yellowish and bluish patches on the weight-spectrum at the third subcarrier. Hence, we conclude that the filter-weights adaptively put stronger blockage on the interference and noise signals along the third subcarrier, at which the target response is the weakest. To confirm this phenomenon further, we devised the Scenario 3 with the strongest target reflectivity along the first subcarrier as  $\Sigma_T^{(3)} = [10, 0.32, 0.06; 0.32, 1, 0.2; 0.06, 0.2, 4]$ . From Fig. 2(c) it is again evident that the filter-weights allow

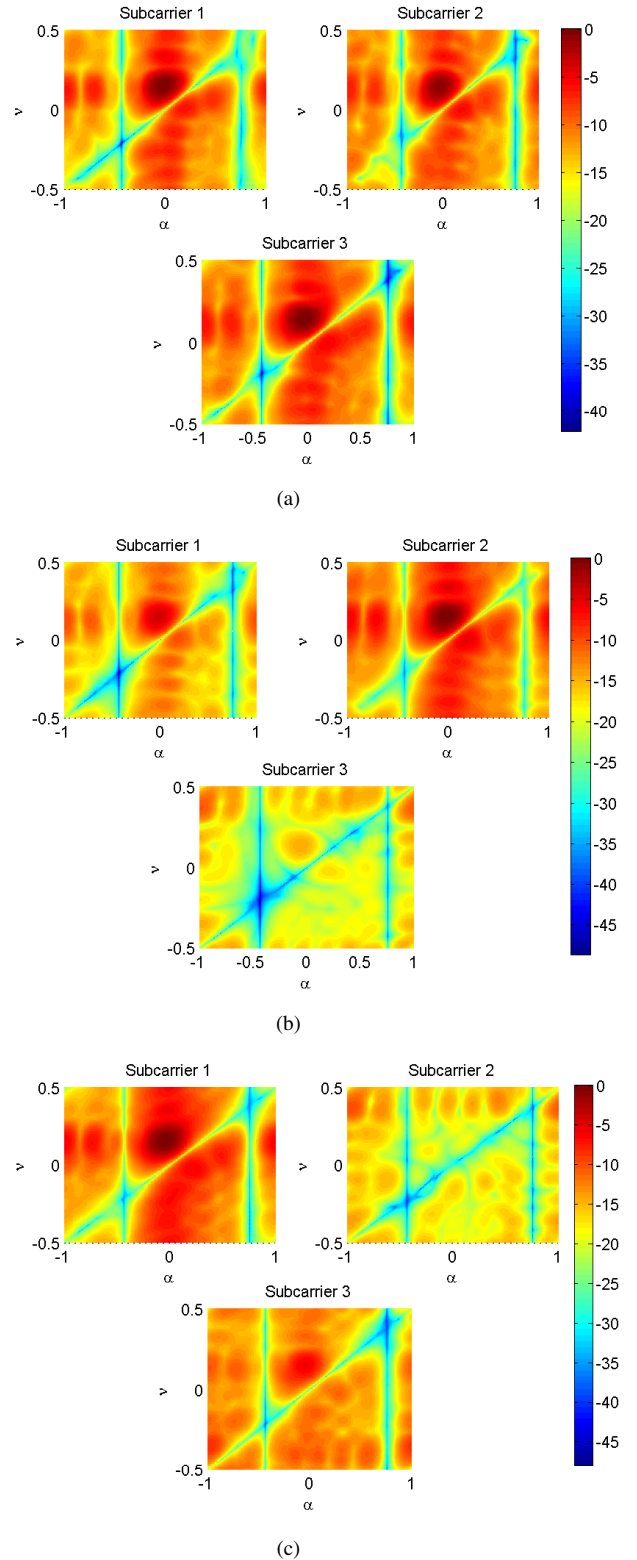


Fig. 2. Spatio-temporal weight spectra at different target scenarios: (a) equal target-reflectivity at all subcarriers, (b) strongest target-reflectivity along the second subcarrier, and (c) strongest target-reflectivity along the first subcarrier. In each subplot, the weight-spectra along the first, second, and third subcarriers are at top-left, top-right, and bottom-middle, respectively.



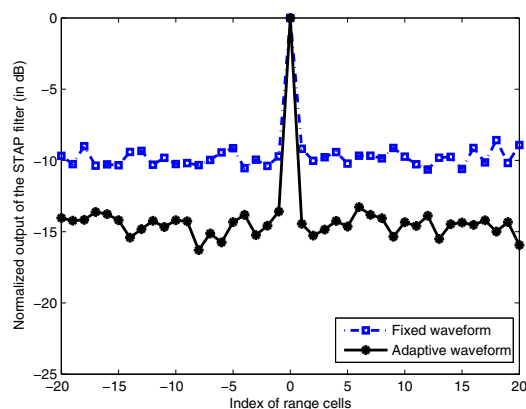


Fig. 3. Performance improvement due to the adaptive waveform design in terms of the normalized outputs of the STAP filter for the Scenario 1.

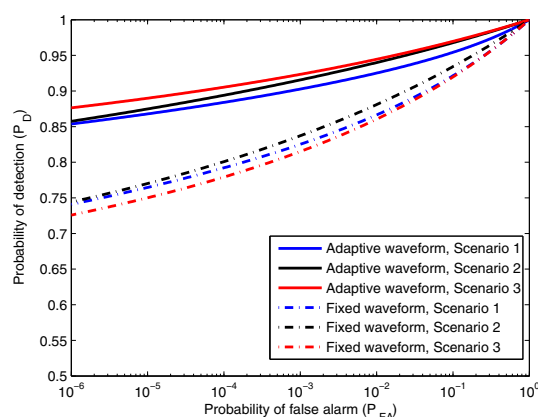


Fig. 4. Performance improvement due to the adaptive waveform design in terms of the receiver operating characteristics.

easy target-detectability along the subcarrier at which the target response is stronger, while simultaneously blocking the interfering signals along some other subcarriers at which the target response is weaker.

In Figs. 3 and 4, we demonstrate the improvement in performance due to the adaptive waveform design technique. For this simulation, we fixed the SNR at 25 dB, while the CNR and JNR values were at 40 dB. Fig. 3 depicts the normalized filter output at different range gates for the Scenario 1 due to the use of adaptive OFDM waveform. To quantify the extent of performance improvement, we plot on the same figure the normalized filter outputs while using the nonadaptive OFDM waveform that transmits  $a_l = 1/\sqrt{L} \forall l$ . It is quite evident that the normalized filter outputs at the secondary gates decrease by approximately 5 dB due to the use of adaptive waveform. From Fig. 4, we also observe similar performance improvement in terms of the receiver operating characteristics. For all the three different target scenarios, the detection probabilities increase by considerable amounts due to the adaptive waveform design. For example, at  $P_{FA} = 10^{-6}$  the adaptive systems show

15–20% of increment in  $P_D$  with respect to their nonadaptive counterparts.

## VI. CONCLUSIONS

In this paper, we proposed an adaptive waveform design technique for an orthogonal frequency division multiplexing (OFDM) radar using a sparsity-based space-time adaptive processing (STAP) technique. The frequency diversity of an OFDM signal improved the target-detectability by adaptively exploiting the frequency-variabilities of the target and interference scenario. We first formulated a realistic sparse-measurement model for OFDM radar considering the effects of both clutter and jammers as the interfering sources. Then, we designed the optimal STAP-filter weight-vector as the generalized eigenvector corresponding to the minimum generalized eigenvalue of the interference and target covariance matrices. Finally, we proposed an adaptive OFDM-waveform design technique and demonstrated the achieved STAP-performance improvement with numerical examples. In future, we will integrate the other waveform design criteria, e.g., ambiguity function and similarity constraint, with the maximum SINR measure, and then design the OFDM coefficients using a multi-objective optimization approach.

## REFERENCES

- [1] L. E. Brennan and I. S. Reed, "Theory of adaptive radar," *IEEE Trans. Aerosp. Electron. Syst.*, vol. AES-9, no. 2, pp. 237–252, Mar. 1973.
- [2] J. Ward, "Space-time adaptive processing for airborne radar," Lincoln Laboratory, Massachusetts Institute of Technology, Lexington, MA, Tech. Rep. 1015, Dec. 1994.
- [3] R. Klemm, *Principles of Space-Time Adaptive Processing*. London, United Kingdom: IET, 2002.
- [4] J. R. Guerci, *Space-Time Adaptive Processing for Radar*. Norwood, MA: Artech House, 2003.
- [5] J. R. Guerci, J. S. Goldstein, and I. S. Reed, "Optimal and adaptive reduced-rank STAP," *IEEE Trans. Aerosp. Electron. Syst.*, vol. 36, no. 2, pp. 647–663, Apr. 2000.
- [6] W. L. Melvin, "A STAP overview," *IEEE Aerosp. Electron. Syst. Mag.*, vol. 19, no. 1, pp. 19–35, Jan. 2004.
- [7] M. C. Wicks, M. Rangaswamy, R. Adve, and T. B. Hale, "Space-time adaptive processing: A knowledge-based perspective for airborne radar," *IEEE Signal Processing Mag.*, vol. 23, no. 1, pp. 51–65, Jan. 2006.
- [8] I. S. Reed, J. D. Mallett, and L. E. Brennan, "Rapid convergence rate in adaptive arrays," *IEEE Trans. Aerosp. Electron. Syst.*, vol. AES-10, no. 6, pp. 853–863, Nov. 1974.
- [9] H. Cox, R. Zeskind, and M. Owen, "Robust adaptive beamforming," *IEEE Trans. Acoust., Speech, Signal Processing*, vol. 35, no. 10, pp. 1365–1376, Oct. 1987.
- [10] B. D. Carlson, "Covariance matrix estimation errors and diagonal loading in adaptive arrays," *IEEE Trans. Aerosp. Electron. Syst.*, vol. 24, no. 4, pp. 397–401, July 1988.
- [11] D. W. Tufts, I. Kirshteins, and R. Kumaresan, "Data-adaptive detection of a weak signal," *IEEE Trans. Aerosp. Electron. Syst.*, vol. AES-19, no. 2, pp. 313–316, Mar. 1983.
- [12] A. M. Haimovich and Y. Bar-Ness, "An eigenanalysis interference canceler," *IEEE Trans. Signal Processing*, vol. 39, no. 1, pp. 76–84, Jan. 1991.
- [13] C. H. Gierull, "Performance analysis of fast projections of the Hung-Turner type for adaptive beamforming," *Signal Processing*, vol. 50, no. 1-2, pp. 17–28, Apr. 1996.
- [14] A. Hoffman and S. M. Kogon, "Subband STAP in wideband radar systems," in *Proc. IEEE Sensor Array and Multichannel Signal Processing Workshop (SAM)*, Cambridge, MA, Mar. 16–17, 2000, pp. 256–260.
- [15] R. Tibshirani, "Regression shrinkage and selection via the lasso," *Jour. of the Royal Statistical Soc. Series B (Methodological)*, vol. 58, no. 1, pp. 267–288, 1996.